Heliyon 10 (2024) e32710

Contents lists available at ScienceDirect

Heliyon

journal homepage: www.cell.com/heliyon

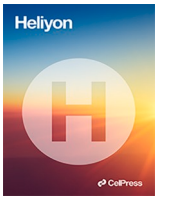

Research article

Molecular dynamics simulation studies on the ionic liquid N-butylpyridinium tetrafluoroborate on the gold surface

Qiang Li [a,b], Guanglai Zhu [a,*], Zhicong Liu [a], Jianqiang Xu [a]

[a] Anhui Province Key Laboratory for Control and Applications of Optoelectronic Information Materials, School of Physics and Electronic Information, Anhui Normal University, Wuhu, 241002, China
[b] Faculty of Engineering, Anhui Sanlian University, Hefei, 230601, China

ARTICLE INFO

Keywords:
Ionic liquid
Solid/liquid interface
Molecular dynamics simulation
Number density

ABSTRACT

The study of solid/liquid interface is of great significance for understanding various phenomena such as the nanostructure of the interface, liquid wetting, crystal growth and nucleation. In this work, the nanostructure of the pyridinium ionic liquid [BPy]BF_4 on different gold surfaces was studied by molecular dynamics simulation. The results indicate that the density of the ionic liquids near the gold surface is significantly higher than that in the bulk phase. Cation's tail (the alkyl chain) orients parallel to the surface under all studied conditions. Cation's head (the pyridine ring) orientation varies from parallel to perpendicular, which depends on the temperature and corrugation of the Au(hkl) surface. Interestingly, analysis of simulated mass and number densities revealed that surface corrugation randomizes the cations packing. On smooth Au(111) and Au(100) surfaces, parallel and perpendicular orientations are well distinguished for densely packed cations. While on corrugated Au(110), cations' packing density and order are decreased. Overall, this study explores the adsorption effect of the gold surface on ionic liquids, providing some valuable insights into their behavior on the solid/liquid interface.

1. Introduction

Ionic Liquids (ILs) are a kind of salt compound with novel properties that exhibit a liquid state at room temperature. They are generally composed of highly asymmetric anions and cations, so the melting point is low. Ionic liquids have the advantages such as extremely low volatility, wide electrochemical window, being miscible with most inorganic and organic compounds, being reusable and environment-friendly [1–3]. As a green solvent that may replace organic solvents, ionic liquids have attracted extensive interest in research. In addition, they are also widely used in many heterogeneous systems, such as lubricants, electro-optic and optoelectronic materials, electrochemistry and fuel cells [4]. The characteristics of the interface structure of ionic liquids on solids often determine the performance of such applications, so it is especially important to explore the structure of ionic liquids on solid surfaces. Therefore, many research groups have carried out studies on the solid-liquid interface properties of ionic liquids [5–10].

As a transition region for the interaction between liquid and solid, the solid-liquid interface has a complex structure. The study of the solid-liquid interface is of great significance for obtaining the nanostructure of the interface and understanding the wetting of the liquid, crystal growth and nucleation [11–13]. Specific single-crystal electrodes with ultra-pure ionic liquids are a new type of electrochemical sensor material, and they have a wide range of applications in surface science and electrochemistry due to their

* Corresponding author.
E-mail address: zhglai@ahnu.edu.cn (G. Zhu).

https://doi.org/10.1016/j.heliyon.2024.e32710
Received 30 December 2023; Received in revised form 26 May 2024; Accepted 7 June 2024
Available online 7 June 2024

advantages, such as a single composition, high purity, good thermal stability, fast electrode response and high sensitivity [14–17]. The properties and applications of ionic liquids are deeply affected by the interface structure. Some research groups have used a variety of experimental methods to study the structure and kinetics of ionic liquids on solid surfaces, such as atomic force microscope, scanning tunneling microscope, Raman spectra, sum frequency spectra, infrared spectra, X-ray diffraction and neutron scattering [18–23]. Mars et al. observed the nanostructure of ionic liquid trifluoromethyl sulfonyl [18] by X-ray reflection and grazing incidence experiments, and observed the ordered structure of alternating layers composed of polar and non-polar units near the surface of the free liquid. Fang et al. studied the properties of Au/ILs solid-liquid interface on the surface of gold electrode and revealed the formation mechanism [23]. Due to the need for high vacuum environment, most surface detection techniques can detect gas-liquid interface, but they are not completely suitable for solid-liquid interface, and molecular simulation technology could overcome this shortcoming.

Therefore, besides experimental studies, there are also a considerable number of theories and simulations to study the Au/ILs interface, in which molecular dynamics (MD) simulation has been widely used to study various interface phenomena. Previous studies have found that water and other liquids form ordered or solid-like layered structures on the substrate of the crystal surface [24]. In the aspect of ionic liquids, Wang et al. used potentiostatic method to compare four different gold force fields and a typical carbon force field system by molecular dynamics simulation [25]. The ion adsorption behavior of the interface between gold electrode and pyrrole ionic liquids was calculated, and the effects of van der Waals interaction, mirror force effect and accumulated ions on the solid-liquid interface were explored. Voroshylova et al. used molecular dynamics simulations to study the effect of different gold surfaces on the differential capacitance of Au(hkl)/ILs interface [26]. It was found that the capacitance of ionic liquid 1-butyl-3-methylimidazolium hexafluorophosphate was relatively high when it was on the rough surface of Au. Sha et al. used molecular dynamics simulations to study the electric double layer structure of single crystalline Au(100) electrode in the ionic liquid 1-butyl-3-methyl-imidazolium hexafluorophosphate [27]. It was found that the structure of the adsorption layer largely determines the maximum zero charge potential and differential capacitance.

These experiments and molecular simulation studies have pointed out that cations and anions in ionic liquids gather orderly on the solid surface in a certain orientation [28]. The transition of ionic liquids from liquids to solids is probably due to the strong interaction between ionic liquids and solid surfaces. In addition to the properties of the liquid, the interaction between the solid surface and the liquid is often closely related to the nanostructure of the surface [29]. Nanostructured gold has the characteristics of high density, high electrical conductivity and excellent biocompatibility [18], so the gold surface has become a widely studied metal nanomaterial and one of the commonly used solid surfaces in self-assembled technology. Compared with imidazolium ionic liquids, there are few studies on the solid-liquid interface of pyridinium ionic liquids, especially on the effects of gold surfaces with different crystal structures on the adsorption and temperature of pyridinium ionic liquids. Therefore, it is of great significance to further study the nanostructure and interaction of pyridinium ionic liquids on the gold surface.

N-butylpyridinium tetrafluoroborate ([BPy]BF_4) is easily soluble in water and completely miscible with most organic solvents. We have previously studied its bulk properties through experimental methods and molecular simulations. In this work, the molecular dynamics simulation method is used to study the structure and order of [BPy]BF_4 on the gold surface, and the effect of temperature on the research results is further compared. The mass density and number density distribution of ionic liquids at Au/ILs interface under different crystal structures are analyzed in detail, and the effect of gold surface with different crystal structures on the arrangement of anions and cations pyridinium ILs is speculated. The results of this work could provide theoretical reference for further experimental study of the nanostructure of ionic liquids on the gold surface.

2. Force field and simulation method

In this work, the ionic liquid is simulated using the all-atom force field developed by Lopes et al. which is based on the OPLS_AA/AMBER force field [30]. With this force field, the bulk properties of [BPy]BF_4 is about 1136 kg/m^3 at 300 K [31], which is in good agreement with the experimental result, with the error less than 2.0 % [32]. The force field parameters for gold are obtained from references [33,34]. The specific expression of the force field of the ionic liquid is shown in formula (1):

$$V_{total} = \sum_{bonds}\frac{k_b}{2}(r-r_{eq})^2 + \sum_{angles}\frac{k_\theta}{2}(\theta-\theta_{eq})^2 + \sum_{angles}\frac{k_\varphi}{2}[1+cos(n\varphi-\delta)] + \sum_{i<j}\left\{4\varepsilon_{ij}\left[\left(\frac{\sigma_{ij}}{r_{ij}}\right)^{12}-\left(\frac{\sigma_{ij}}{r_{ij}}\right)^{6}\right]+\frac{q_i q_j}{4\pi\varepsilon_0 r_{ij}}\right\} \quad (1)$$

The total energy of the system is expressed by V_{total}, which includes five parts: bond length, bond angle, dihedral angle, van der Waals interaction and electrostatic interaction. Firstly, three gold surfaces are constructed. Au(100) and Au(111) are composed of three layer 21 × 21 slab of 1323 Au atoms, and Au(110) is composed of three layer 21 × 15 slab of 945 Au atoms. The final size of Au (100) and Au(111) surfaces is 6.06 × 6.06 nm^2, while that of the Au(110) surface is 6.12 × 6.06 nm^2. Then, a pure [BPy]BF_4 system consisting of 800 ion pairs is constructed by using the simulation software Packmol [35], which is placed in a box of 6 × 6 × 6 nm^3 to minimize the energy, and then a molecular dynamics simulation is carried out for 20 ns under the NPT ensemble by using Gromacs 5.1.4 [36]. Finally, the obtained pure [BPy]BF_4 system is placed on gold surfaces along the Z direction, respectively. The gold surface is parallel to the XY direction, and the Z-axis direction is the normal direction of the surface. The distance between the ionic liquid and the gold surface is about 0.2 nm.

The final system consists of 800 ion pairs and a gold surface with triple layers of gold sheets, as shown in Fig. 1. At the same time, in order to avoid the influence of periodic boundary conditions, we have extended the Z direction of all boxes to 15 nm. In this way, two

rectangular box configurations with a box size of 6.06 × 6.06 × 15 nm^3 and a rectangle box of 6.12 × 6.06 × 15 nm^3 are formed. After the energy minimization, simulations for 50 ns have been carried out under the NVT ensemble, and the last 5 ns trajectory is adopted for analysis. In the process of simulation, three temperatures are set at 300 K, 500 K and 700 K, the simulation step time is set to 2 fs, and every 0.2 ps is sampled. All the simulations are under the periodic boundary conditions, with cut-off radius of 1.3 nm used for the coulombic interactions. The temperature of the system is controlled using V-rescale method. The long-range electrostatic interaction is treated by PME method, and the bond length constraint is treated by LINCS algorithm.

3. Results and discussion

3.1. Mass density distribution of ionic liquids on gold surfaces

Firstly, the effect of gold surface with different crystal structures on the distribution of pyridinium ionic liquids was studied. Fig. 2 and Fig. S1 show the total mass density of [BPy]BF_4 at 300 K and the mass density distribution of corresponding anions and cations along the Z-axis on the surfaces of Au(100), Au(110) and Au(111). From the total mass density shown in Fig. 2(a), it can be seen that the pyridinium ionic liquid has a dense layer configuration on the surface of Au(100), and its density is much higher than that of the bulk phase of the ionic liquid. Afterwards, another three peaks, which are significantly lower than the dense layer can be observed, and then the mass density of ionic liquids tends to be stable, indicating that as the ionic liquids become farther and farther away from the surface of Au(100), the effect of this surface on ionic liquids becomes smaller and smaller, and finally tends to the ionic liquid bulk phase.

The corresponding mass density distribution of anions and cations is presented in the illustration of Fig. 2(a). It can be seen that the contribution of anions and cations to the mass density of ionic liquids on the gold surface is obviously different. In the first dense layer formed on the surface of Au(100), the maximum mass density of the ionic liquid at z = 0.74 nm is 5182.2 kg/m^3, of which cations (4254.4 kg/m^3) account for about 4/5, while the second peak is mainly contributed by anions. It can be seen that the cations formed on the surface of Au(100) account for the main contribution. The anions at the corresponding position of the second peak formed by cations on the surface of Au(100) also correspond to two peaks. It can be inferred that most of the cations in the aggregation layer tend to lie flat on the Au surface [37], which is related to the strong adsorption of ionic liquids on the Au(100) surface, which will be described in more detail by number density and angle analysis.

In order to further understand the effect of gold surfaces with different crystal structures on the structural distribution of ionic liquids, we further analyzed the mass distribution of [BPy]BF_4 and its corresponding anions and cations along the Z-axis on the surfaces of Au(110) and Au(111) at 300 K. Fig. 2(b) shows the total mass density distribution of [BPy]BF_4 on the surface of Au(110). It can be seen that the dense layer of ionic liquids is also formed on the surface of Au(110). The difference is that the height of this dense layer is significantly lower than that of the Au(100) surface. A relatively low and less obvious peak is produced between the first two obvious ones, which is related to the different interaction between anions and cations and the surface [38,39]. Fig. 2(b) also shows the mass distribution of anions and cations on the Au(100) surface, which is different from that on Au(100). Although the distribution of anions and cations tends to be stable, there is a clear oscillation behavior, and the distribution range of anions in the first dense layer is wider than that of cations, which is related to the effect of Au(110) surface on ionic liquids. Similarly, the contribution of cations to mass

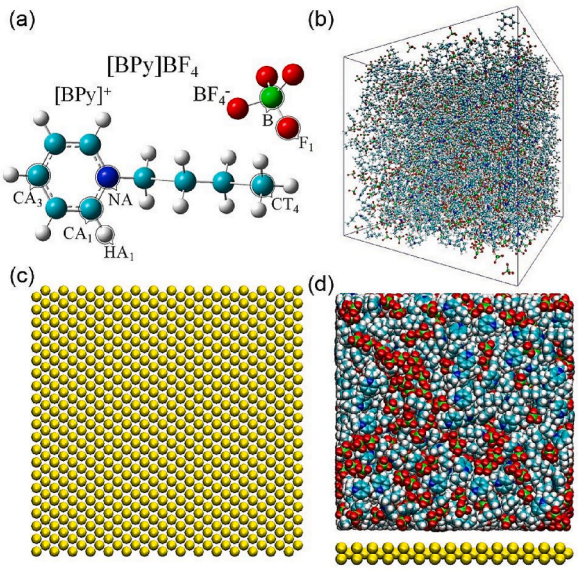

Fig. 1. (a) Structure of [BPy]BF_4; (b) System of [BPy]BF_4; (c) Gold surface; (d) [BPy]BF_4 on the gold surface. (For interpretation of the references to colour in this figure legend, the reader is referred to the Web version of this article.)

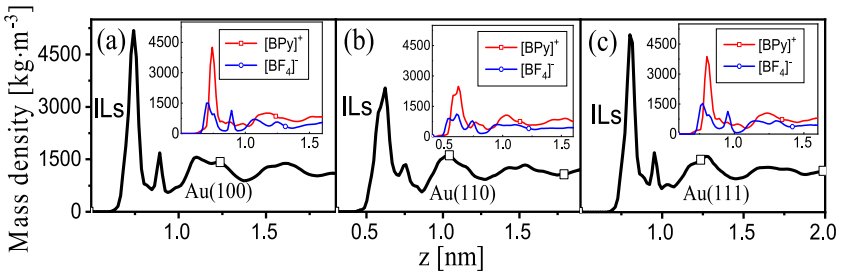

Fig. 2. Mass density distribution of $[BPy]BF_4$ along the Z-axis and the inset showing the corresponding anion and cation on Au surfaces at 300 K. (a) Au(100); (b) Au(110); (c) Au(111).

density is greater than that of anions.

Fig. 2(c) shows the total mass distribution of $[BPy]BF_4$ on the surface of Au(111). It can be observed that a peak of mass density formed by $[BPy]BF_4$ on the surface of Au(111) is almost the same as the first peak formed on the surface of Au(100). This is because the surfaces of both Au(100) and Au(111) are smooth. The mass distribution of anions and cations of $[BPy]BF_4$ on Au(111) surface is shown in the illustration of Fig. 2(c) Compared with Au(100) surface, we can find that the effect of Au(100) and Au(111) on anions and cations is almost the same, which is due to the small difference in nanostructure between Au(100) surface and Au(111) surface.

3.2. Number density distribution of some atoms on cations

In order to study the distribution of the head and tail of cations on the gold surface more clearly, we performed the number density analysis, which is more conducive to understanding the nanostructure of the dense layer [40]. The number densities and corresponding positions of the nitrogen atom NA and the adjacent carbon atom CA1 on the cationic pyridine ring can be used to speculate the distribution of the head of the cation. And the carbon atom CT4 at the end of the alkyl chain can be used to observe the tail distribution of the cation. Fig. 3 shows the number density distribution of some representative atoms on the cations on the Au(100) surface along the Z-axis. It can be seen that near the Au(100) surface, the number density of CT4 is the highest, that of NA the second, and that of CA1 is the smallest. After the main peak of number densities, the secondary peaks of atomic number density such as NA, CA1 and CT4 can also be observed. The value of each sub-peak is much lower than that of the first peak, and the position of the peak also changes. The sub-peak of the NA atom is first observed, followed by the CA1 atom, and finally the CT4 atom at the end of the alkyl chain.

According to the above observation results, it can be inferred that the distribution of cationic $[BPy]^+$ on the Au(100) surface is characterized by the fact that most of the tails are parallel to the surface, while the arrangement of the head is slightly random. From the distribution of the secondary peak, it can be inferred that the plane of the pyridine ring at the head of the cation is not completely parallel to the surface of Au(100). To illustrate this point, we give a snapshot of the aggregation layer of ionic liquids at a distance of 0.6 nm from Au(100). As is clearly shown in Fig. 4, most of the alkyl chains tend to lie parallel to the surface, while for the pyridine rings, some lie flat, and the others are randomly distributed at certain angle to the Au (100) surface. This will be further discussed by angle distribution in section 3.3.

Fig. 5 shows the number density distribution of some representative atoms on the cations on the Au(110) surface along the Z-axis. It can be seen that the number density of CT4 atoms on the surface is the highest, followed by NA atoms, and finally CA1 atoms. Different from the distribution of these atoms on the surface of Au(100), the positions of the number density peaks of the three atoms are also different. The first is the CT4 atom, the second is the CA1 atom with the lowest number density, and the last is the NA atom. After each main peak, we also observe the second peak of the number density, which is opposite to the law of the main peak. The number of CT4

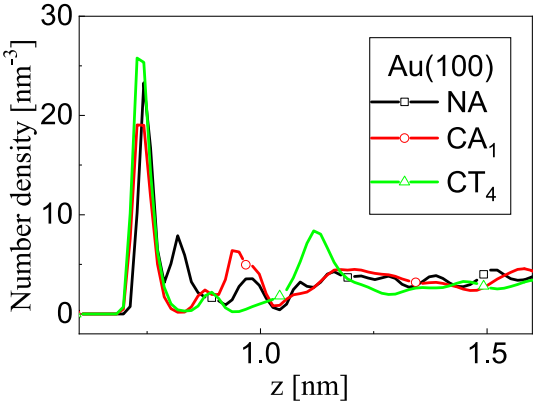

Fig. 3. The number density distribution of the upper atoms of [BPy]BF4 cations at 300 K along the Z-axis on Au (100) surface.

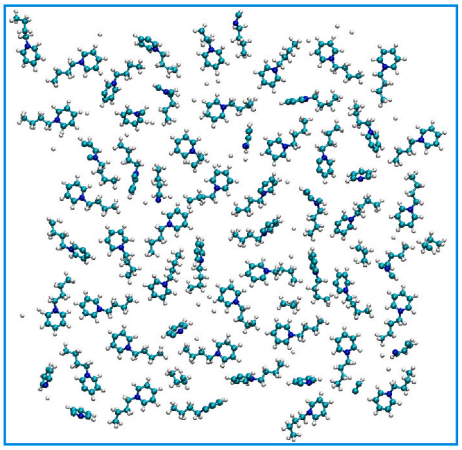

Fig. 4. A snapshot of the distribution of cations of [BPy]BF_4 near Au(100) at 300 K.

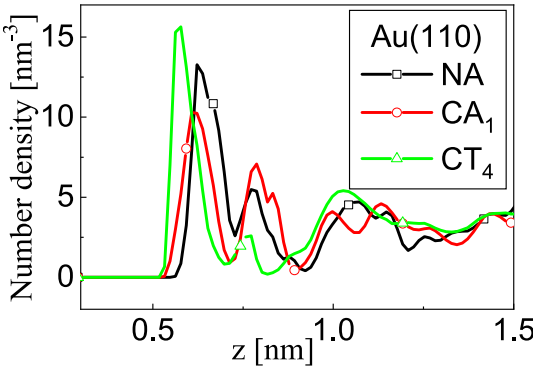

Fig. 5. The number density distribution of the upper atoms of [BPy]BF4 cations at 300 K along the Z-axis on Au (110) surface.

atoms is the smallest, that of the NA atoms the second, and that of the CA1 atoms is the largest, and they are located in the same position. Through the above analysis, it can be predicted that there are a large number of tails of cations on the surface of Au(110), and the head is slightly away from the surface relative to the tail. Furthermore, the heads of most cations are perpendicular to the Z-axis, equivalent to the plane where the pyridine ring is located parallel to the Au(110) surface.

Finally, the number density distributions of some representative atoms on the Au(111) surface are shown in Fig. 6. It can be seen that the first number density peaks of the above three atoms all appear in the same position, which is consistent with our previous conclusion that both the Au(100) surface and the Au(111) surface have similar effects on the pyridinium ionic liquid [BPy]BF_4. Similarly, the second number density peaks of NA, CA1 and CT4 also appear in turn.

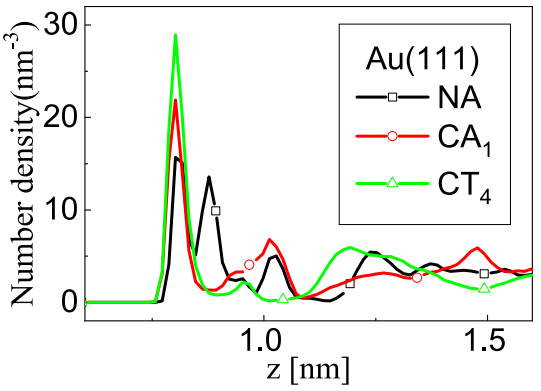

Fig. 6. The number density distribution of the upper cations of [BPy]BF4 on the Au (111) surface at 300 K along the Z-axis.

Through the number density analysis of some representative atoms of cations along the Z-axis, we can draw a conclusion: The cations of the pyridinium ionic liquids gather adjacent to the gold surfaces and most of them lie flat on the surface. The difference is that the number density of the representative atoms on Au(110) is significantly lower than that on Au(100) and Au(111) surfaces. Moreover, the tails of cations gather closer to the Au(110) surface than the heads of them.

In order to more clearly compare the difference between the nonstructural layer near the surface and the liquid phase region, we also give the radial distribution functions (RDFs) of the characteristic atoms in these two regions [41–43]. As shown in Fig. S2 in Supporting Information, the RDFs peak value at the interface is much higher than that in the liquid phase region under all conditions, indicating that the adsorption of the surface increases the order of ionic liquids. For all three surfaces, as shown in Fig. 7, the RDFs of the head (HA1-F) are similar, while the RDFs value of the tail (CT4-CT4) on Au(110) is much lower than that on the other two surfaces, indicating that the influence of the Au(110) surface on the tail is more significant, which is consistent with the number density analysis.

3.3. Angle distribution of cations on the surfaces

In order to further explore the distribution character of the pyridine ring of cations on the gold surfaces, we have made the probability distribution of the angle (θ_{ring}) between the normal direction of the pyridine ring of cation and the normal direction of the gold surfaces (the direction along Z-axis). At the same time, the angle (θ_{alkyl}) between the alkyl chain of cation (the vector from atom NA to CT4) and the Z-axis was made as a comparison. The schematic diagram about the angle distribution can be referred to Fig. 8.

We define the maximum peak on the density distribution of ionic liquids as the first layer to study the orientation distribution of cations on the gold surface. Specifically, the first layer is determined by the first lowest density position after the maximum peak. For example, the boundary of the first layer of ILs on Au(100) is $z < 0.9375$ nm. The difference in the boundary of the first layer surfaces is mainly due to the different structures that determine the heights of the three gold surfaces.

As shown in Fig. 9(a), it can be seen that the pyridine rings have obvious orientation distributions. For Au(100) and Au(111), most of the distribution is in the range of 0°∼30° and 150°∼180°, indicating that the pyridine rings are more likely to lie flat on the gold surface. In addition, the part of pyridine rings are also distributed between 60° and 120°. For Au(110), the probabilities in 0°∼30° (150°∼180°) and 60°∼120° intervals are roughly equal, indicating that half of the pyridine rings tending to lie flat on the gold surface, while the other half standing upright on the surface.

For the three gold surfaces, the angle between the alkyl chain and the Z-axis is mainly concentrated between 80° and 100° (Fig. 9 (b)), indicating that the tails of cations tend to be arranged parallel to the gold surface. The overall distribution on the three gold surfaces is similar. However, the distribution on Au(110) is more concentrated, and the orientation distribution of the alkyl chains is wider, indicating that the surface type also has a certain impact on the orientation of the alkyl chain. This is similar to the distribution of the alkyl chain of the imidazolium ionic liquid on the gold surface [44].

The above analysis supports our previous conclusion that the cations of the pyridinium ionic liquid gather near the gold surfaces and mainly lie flat on the surface. The tails tend to be arranged parallel to the gold surface. The distribution of pyridine rings on the three surfaces is slightly different. Specially, the distribution probability on Au(110) is more extensive. This is due to the different interaction between ILs and Au(110), which has a atomically corrugated surface, leading the pyridine ring fall to the grooves on the surface [45].

3.4. Effect of temperature on the ionic liquids on gold surfaces

Temperature will have a great influence on the nanostructure of ionic liquids on the solid surface [46]. The study in this aspect is also helpful to understand the properties of solid-liquid interface. Fig. 10 and Fig. S3 show the total mass density distribution along the normal direction of ionic liquids [BPy]BF_4 on Au(100), Au(110) and Au(111) surfaces at different temperatures. It can be seen that with the increase of temperature, both the mass density of the dense layer on the surface and the bulk phase density of the ionic liquids behind the layer decrease. The effect of temperature on the total mass density is obvious. The decrease of the dense layer indicates that the increase of temperature makes the uneven aggregation of ionic liquids smaller and the structure relatively loose, which greatly reduces the heterogeneity of the ionic liquids. It can also be seen from Fig. 10 that the mass density of ionic liquids at 700 K tends to be stable after several peaks, which indicates that with the increase of the distance to the surface, the interaction between the gold surface and ionic liquids can be almost ignored, and the system reaches bulk phase equilibrium.

Through the above analysis of the mass density of [BPy]BF_4 on the gold surface at different temperatures and different gold

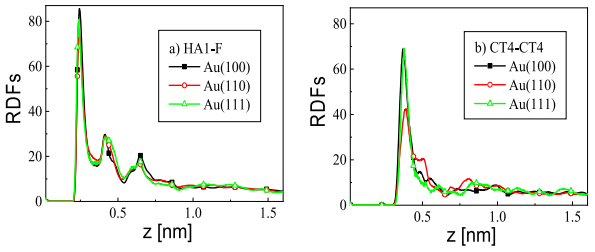

Fig. 7. Radial distribution functions of the cation's characteristic atoms: a) Head (HA1-F); b) Tail (CT4-CT4).

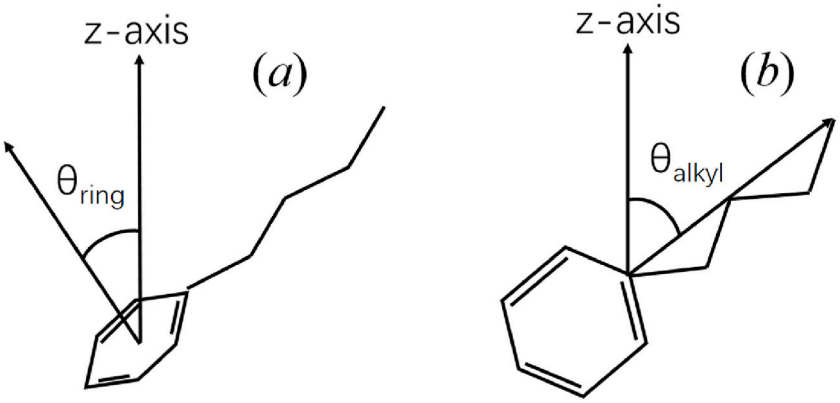

Fig. 8. A schematic diagram of the angle distribution of cation: (a) θ_{ring} represents the angle between the normal direction of the pyridine ring and the Z-axis; (b) θ_{alkyl} represents the angle between the alkyl chain and the Z-axis.

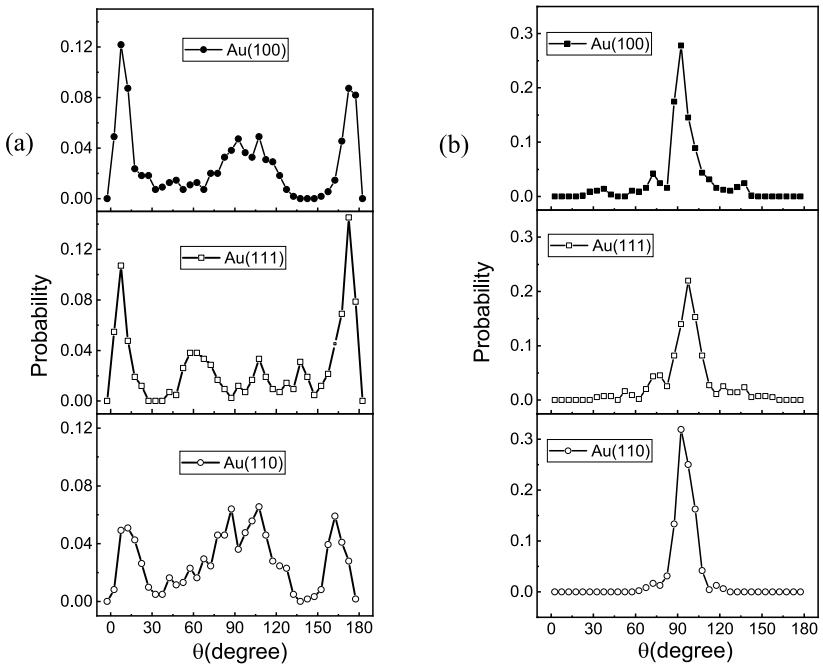

Fig. 9. (a) θ_{ring}, (b) θ_{alkyl} of cations of the first layer on Au(100), Au(111) and Au(110) surfaces.

surfaces, we can draw a conclusion that there are similar laws on Au(100), Au(111) and Au(110) surfaces, that is, the mass density of pyridinium ionic liquids on the gold surface decreases with the increase of temperature. However, the position of the Z-axis corresponding to the peak of the mass density is almost unchanged. The mass density on the Au(110) surface fluctuates greatly, which is related to the great difference in the properties between the Au(110) surface and the other two surfaces discussed earlier.

To help in rationalizing orientation of cations of $[BPy]BF_4$ on the Au surfaces, the more comprehensive number density distributions including the position of anions, have been provided as Figs. S4–S6 in Supporting Information. The snapshot with anions has been also provided in Fig. S7. We can see that a anion laying is presented on the surface, which indicates pyridinium cations have a distinct ability to coordinate anions. Except the angular distribution, the pyridine rings standing perpendicular to the Au(110) surface could be supported by a more obvious anion laying at the surface which is shown by the B atoms distribution in Fig. S5.

3.5. Discussion

In according with some works on Au(hkl)-imidazolium ionic liquid interfaces [45,47], $[BPy]BF_4$ shows a strong layering near the surface and the tail tends to be parallel to the surface. This phenomenon also exists at other metal interfaces, for example, experiments have confirmed that another similar pyridinium ionic liquid $[BMPy]BF_4$ (1-butyl-4-methylpyridinium tetrafluoroborate) at the Bi(111)

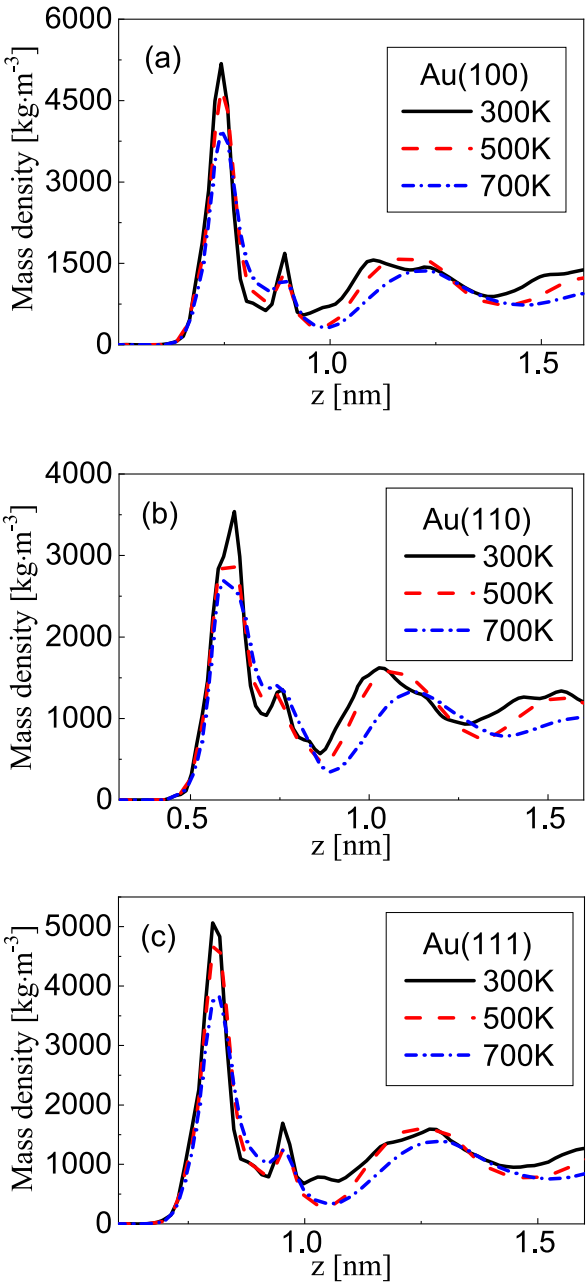

Fig. 10. Mass density distributions of [BPy]BF_4 on the gold surfaces along the Z-axis at different temperatures (a) Au(100); (b) Au(110); (c) Au (111). (For interpretation of the references to colour in this figure legend, the reader is referred to the Web version of this article.)

surface can form a multilayer structure [48]. How to explain this phenomenon? The energy when the tail is parallel to the surface is lowest. If we assume the tail is perpendicular, then $[BPy]^+$ cation must stand on H–C bond(s), like a ballerine, which is energetically hard. Therefore, most of tails are parallel to the surface.

Meanwhile, we can see the surfaces do not seem to have obvious effect on the angular distribution orientation of the tails from Fig. 9. The RDFs results show that the order of head and tail is significantly increased in the nanostructure regions, indicating that both heads and tails of pyridinium cations can take orientations on the gold surface. This is similar to the effect of the imidazolium ionic liquid with a solid surface. It has been affirmed that imidazolium heads and tails can take both orientations by plenty of MD and experimental data [49–52]. For example, Maier et al. found that the imidazolium cations are adsorbed in a flat geometry on the Au (111) surface (<0.5 ML coverage) [49]. The difference is that, in this work, pyridinium cations are parallel to the surface for pure [BPy] BF_4.

In addition to well-studied imidazolium-based ionic liquids, we have studied another important ionic liquid family, pyridinium-

based, on the surface of gold. For all three gold surfaces, the tails of pyridinium cations lie parallel to the surface. The remarkable feature of these cations to keep their neutral tails on the surface should affect the relative permittivity, resulting in decreasing capacitance. The same feature could be essential for sensors due to increased adsorption selectivity. These conclusions call for computational and experimental confirmation.

4. Conclusions

In this work, the effects of the gold surface with different crystal structures and temperature on the distribution of N-butylpyridinium tetrafluoroborate ([BPy]BF_4) were studied by molecular dynamics simulation. The mass density results show that the ionic liquids will form a dense layer on their surfaces, and the smooth surfaces of Au(100) and Au(111) have similar effects on [BPy]BF_4. Although the dense layer of ionic liquids is also produced on the rough surface of Au(110), the nanostructure order of ionic liquids near the surface decreases, which is different from that of Au(100) and Au(111) surfaces. Furthermore, the tails (alkyl chains) of cation tend to be parallel to the surface, while some of the heads (pyridine rings) lie flat on the surface and the others are randomly distributed. Increasing temperature does not affect the distance of ILs' closest approach to the surface, yet expectedly loses the packing density of ILs.

Data availability statement

Data will be made available on request.

CRediT authorship contribution statement

Qiang Li: Writing – original draft, Visualization, Validation, Methodology, Investigation, Data curation. **Guanglai Zhu:** Writing – review & editing, Writing – original draft, Supervision, Project administration, Methodology, Investigation, Funding acquisition, Data curation, Conceptualization. **Zhicong Liu:** Writing – original draft, Visualization, Methodology. **Jianqiang Xu:** Visualization, Writing – original draft.

Declaration of competing interest

The authors declare that they have no known competing financial interests or personal relationships that could have appeared to influence the work reported in this paper.

Acknowledgments

This work was supported by Anhui Provincial Natural Science Foundation (No. 2108085MA21) and National Natural Science Foundation of China(No. 21173002). The authors express their gratitude to the reviewers for their valuable insights on data analysis and scientific writing, which have significantly enhanced the overall quality of the manuscript.

Appendix A. Supplementary data

Supplementary data to this article can be found online at https://doi.org/10.1016/j.heliyon.2024.e32710.

References

[1] R.D. Rogers, K.R. Seddon, Science 302 (2003) 792–793.
[2] R. Hayes, G.G. Warr, R. Atkin, Chem. Rev. 115 (2015) 6357–6426.
[3] T.A. Lima, V.H. Paschoal, L.F.O. Faria, M.C. Ribeiro, C. Giles, J. Chem. Phys. 144 (2016) 224504.
[4] I. Osada, H. de Vries, B. Scrosati, S. Passerini, Angew. Chem., Int. Ed. 55 (2016) 500–513.
[5] Y. Lauw, M.D. Horne, T. Rodopoulos, A. Nelson, F.A. Leermakers, M. J. Phys. Chem. B 114 (2010) 11149–11154.
[6] J. Vatamanu, O. Borodin, G.D. Smith, J. Am. Chem. Soc. 132 (2010) 14825–14833.
[7] G. Feng, J.S. Huang, B.G. Sumpter, V. Meunier, R. Qiao, Phys. Chem. Chem. Phys. 13 (2011) 14723–14734.
[8] P. Wu, J.S. Huang, V. Meunier, B.G. Sumpter, R. Qiao, ACS Nano 5 (2011) 9044–9051.
[9] Q.Q. Dong, H.B. Hu, S.Q. Chen, Q. He, L.Y. Bao, Acta Phys. Sin. 67 (2018) 054702.
[10] C. Merlet, B. Rotenberg, P.A. Madden, P. Taberna, P. Simon, Y. Gogotsi, M. Salanne, Nat. Mater. 11 (2012) 306–310.
[11] Y. Sun, G. Xie, Y. Peng, W. Xia, J. Sha, Colloid. Surface. 495 (2016) 176–186.
[12] D. Zhang, S. Takase, G. Nagayama, J. Colloid Interface Sci. 591 (2021) 474–482.
[13] V. Gómez-González, B. Docampo-Álvarez, J.M. Otero-Mato, O. Cabeza, L.J. Gallego, L.M. Varela, Phys. Chem. Chem. Phys. 20 (2018) 12767–12776.
[14] S. Maruyama, Y.J. Matsumoto, J. Phys. Chem. C 119 (2015) 17755–17761.
[15] A.V. Rudnev, M.R. Ehrenburg, E.B. Molodkina, A. Abdelrahman, M. Arenz, P. Broekmann, T. Jacob, Chemelectrochem 7 (2020) 501–508.
[16] T. Uemura, R. Hirahara, Y. Tominari, S. Ono, S. Seki, J. Takeya, Appl. Phys. Lett. 93 (2008) 263305.
[17] S. Koshizawa, Y. Katayama, T. Miura, Electrochim 77 (2009) 627–629.
[18] R. Wen, B. Rahn, O.M. Magnussen, Angew. Chem., Int. Ed. 54 (2015) 6062–6066.
[19] Z.C. Huang, Y.Z. Dai, X.J. Wen, D. Liu, Y.X. Lin, Z. Xu, J. Pei, K. Wu, Acta Phys. Chim. Sin. 36 (2020) 1907043.

[20] M.G. Li, L. Chen, Y.X. Zhong, Z.B. Chen, J.W. Yan, B.W. Mao, Electrochim. Acta 197 (2016) 282–289.
[21] H.W. Cheng, P. Stock, B. Moeremans, T. Baimpos, X. Banquy, F.U. Renner, M. Valtiner, Adv. Mater. Interfac. 2 (2015) 1500159.
[22] J. Mars, B. Hou, H. Weiss, H. Li, O. Konovalov, S. Festersen, M. Mezger, Phys. Chem. Chem. Phys. 19 (2017) 26651–26661.
[23] S. Wang, Y. Tu, R. Wan, H. Fang, J. Phys. Chem. B 116 (2012) 13863–13867.
[24] A. Srivastava, J. Hassan, D. Homouz, Molecules 26 (2021) 6175.
[25] R. Wang, S. Bi, V. Presser, G. Feng, Fluid Phase Equil. 463 (2018) 106–113.
[26] I.V. Voroshylova, M. Lembinen, H. Ers, M. Mišin, V.A. Koverga, C.M. Pereira, M.N.D. Cordeiro, Electrochim. Acta 318 (2019) 76–82.
[27] M. Sha, Q. Dou, F. Luo, G. Zhu, G. Wu, ACS Appl. Mater. Interfaces 6 (2014) 12556–12565.
[28] M. Wagstaffe, M.J. Jackman, K.L. Syres, A. Generalov, A.G. Thomas, ChemPhysChem 17 (2016) 3430–3434.
[29] S. Wang, Y.S. Tu, R.Z. Wan, H.P. Fang, Commun. Theor. Phys. 59 (2013) 623–628.
[30] J.N.C. Lopes, A.A.H. Pádua, J. Phys. Chem. B 110 (2006) 19586–19592.
[31] G. Zhu, X. Kang, S. Zhou, X. Tang, M. Sha, Z. Cui, X. Xu, RSC Adv. 7 (2017) 4896–4903.
[32] B. Mokhtarani, A. Sharifi, H.R. Mortaheb, M. Mirzaei, M. Mafi, F. Sadeghian, J. Chem. Thermodyn. 41 (2009) 323–329.
[33] H. Heinz, R.A. Vaia, B.L. Farmer, R.R. Naik, J. Phys. Chem. C 112 (2008) 17281–17290.
[34] Y.L. Wang, M. Golets, B. Li, S. Sarman, A. Laaksonen, ACS Appl. Mater. Interfaces 9 (2017) 4976–4987.
[35] L. Martínez, R. Andrade, E.G. Birgin, J.M. Martínez, J. Comput. Chem. 30 (2009) 2157–2164.
[36] M.J. Abraham, T. Murtola, R. Schulz, S. Páll, J.C. Smith, B. Hess, E. Lindahl, SoftwareX 1 (2015) 19–25.
[37] R. Yamamoto, H. Morisaki, O. Sakata, H. Shimotani, H. Yuan, Y. Iwasa, T. Kimura, Y. Wakabayashi, Appl. Phys. Lett. 101 (2012) 053122.
[38] M. Bahrami, M.H. Ghatee, S.F. Ayatollahi, J. Phys. Chem. B 124 (2020) 2835–2847.
[39] S.F. Ayatollahi, M. Bahrami, M.H. Ghatee, T. Ghaed-Sharaf, Ind. Eng. Chem. Res. 59 (2020) 16258–16272.
[40] C. Liu, Z. Yu, D. Neff, A. Zhamu, B.Z. Jang, Nano Lett. 10 (2010) 4863–4868.
[41] K. Okuwaki, Y. Mochizuki, H. Doi, S. Kawada, T. Ozawa, K. Yasuoka, RSC Adv. 8 (2018) 34582–34595.
[42] Y. Kawagoe, G. Kikugawa, K. Shirasu, T. Okabe, Soft Matter 17 (2021) 6707–6717.
[43] Y. Kawagoe, D. Surblys, H. Matsubara, G. Kikugawa, T. Ohara, Langmuir 36 (2020) 6482–6493.
[44] Y. Wang, G. Tian, Langmuir 37 (2021) 14059–14071.
[45] I.V. Voroshylova, M. Lembinen, H. Ers, M. Misin, V.A. Koverga, C.M. Pereira, V.B. Ivanistsev, M.N.D.S. Cordeiro, Electrochim. Acta 318 (2019) 76–82.
[46] C. Zhang, X. Li, J.S. Wang, J. Phys. Chem. C 123 (2019) 18914–18923.
[47] E.S.C. Ferreira, C.M. Pereira, M.N.D.S. Cordeiro, D.J.V.A. Santos, J. Phys. Chem. B 119 (2015) 9883–9892.
[48] E. Anderson, V. Grozovski, L. Siinor, C. Siimenson, V. Ivanistev, K. Lust, S. Kallip, E. Lust, J. Electroanal. Chem. 709 (2013) 46–56.
[49] T. Cremer, M. Stark, A. Deyko, H.P. Steinruck, F. Maier, Langmuir 27 (2011) 3662–3671.
[50] J.Y. Fu, X.C. Li, Z. Yu, X.N. Huang-Fu, J.A. Fan, Z.Q. Zhang, S. Huang, J.F. Zheng, Y.H. Wang, X.S. Zhou, Langmuir 38 (2022) 6209–6216.
[51] N. Sieffert, G. Wipff, J. Phys. Chem. C 112 (2008) 19590–19603.
[52] S.D. Lecce, A.A. Kornyshev, M. Urbakhb, F. Bresme, Phys. Chem. Chem. Phys. 23 (2021) 22174–22183.